THE ASTRONOMICAL JOURNAL VOLUME 110, NUMBER 4 OCTOBER 1995

MEASURING THE HUBBLE CONSTANT WITH THE *HUBBLE SPACE TELESCOPE*[1,2]

ROBERT C. KENNICUTT, JR.
Steward Observatory, University of Arizona, Tucson, Arizona 85721
Electronic mail: robk@as.arizona.edu

WENDY L. FREEDMAN
Carnegie Observatories, 813 Santa Barbara St., Pasadena, California 91190
Electronic mail: wendy@ociw.edu

JEREMY R. MOULD
Mt. Stromlo & Siding Spring Observatories, Institute of Advanced Studies, Australian National University, Weston Creek P.O., ACT 2611, Australia
Electronic mail: jrm@mso.anu.edu.au

Received 1995 June 8

ABSTRACT

The spectacular success of the *Hubble Space Telescope* (*HST*) repair mission now makes it possible to realize one of the astrophysical goals for which the *HST* was designed. Despite recent progress in ground-based measurements of the distance scale, the value of the Hubble constant remains uncertain at the $\pm 20\%$–30% level. The incompatibility of high values of H_0 with the stellar age scale in an Einstein–de Sitter universe underscores the need for a definitive calibration of the distance scale. This paper briefly reviews the current status of the distance scale calibration, and describes ongoing programs to measure H_0 with *HST*, with special emphasis on the Extragalactic Distance Scale Key Project. The objective of the Key Project is to combine *HST* observations of Cepheid variables in ~25 galaxies with ground-based observations of five secondary distance indicators to measure H_0 to an accuracy of $\pm 10\%$. The sample selection, observing strategy, data analysis methods, and error budget are designed to minimize susceptibility to the kinds of systematic errors which have often plagued distance scale determinations. The successful measurement of Cepheids in the Virgo cluster spiral M100 demonstrates the feasibility of this program, and already constrains H_0 to the range 80 ± 17 km s^{-1} Mpc^{-1}. The ultimate goal of measuring H_0 to $\pm 10\%$ awaits successful completion of the Key Project over the next three years. © *1995 American Astronomical Society.*

1. INTRODUCTION

"The distance scale path has been a long and tortuous one, but with the imminent launch of HST there seems good reason to believe that the end is finally in sight."
Marc Aaronson (1985 Pierce Prize Lecture)

From its inception the *Hubble Space Telescope* (*HST*) was designed to measure the expansion rate of the universe to unprecedented accuracy (e.g., National Academy of Sciences 1969). This objective was formalized in 1987 when the calibration of the distance scale was chosen as one of the three *HST* Key Projects, with the explicit target of determining H_0 to an accuracy of $\pm 10\%$. Progress in this program was delayed by the spherical aberration problem, but with the recent refurbishment of *HST* Aaronson's goal once again is in sight.

This paper reviews recent progress in the calibration of the distance scale and describes the ongoing *HST* programs, with emphasis on the Key Project. We begin with a brief review of recent ground-based observations, focussing especially on the secondary distance ladder, which forms a vital part of the Key Project (Sec. 2). This discussion draws heavily on recent reviews by Jacoby *et al.* (1992), van den Bergh (1992), de Vaucouleurs (1993), and Sandage & Tammann (1995), and we refer the reader to those papers for more complete discussions and a full range of viewpoints on this controversial subject. Section 3 addresses the issue of how accurately H_0 is known at present, why various estimates of H_0 (and its uncertainty) are so discrepant, and how *HST* observations should resolve this problem. Section 4 describes the strategy and design of the *HST* Key Project, and Sec. 5 summarizes some preliminary results from the first year of this three-year program.

The Key Project is a large collaborative effort, and the results presented in Secs. 4 and 5 are due to the contributions of numerous team members. Co-Investigators on the project are S. Faber, H. Ford, W. Freedman (Co-PI), J. Graham, J. Gunn, J. Hoessel, J. Huchra, S. Hughes, G. Illingworth, R.

[1]Based on invited talks given at the 185th meeting of the American Astronomical Society.
[2]EDITOR'S NOTE: The *Astronomical Journal* has a long-standing tradition of publishing occasional review papers. In the past these have often been based, as is this one, on invited talks presented at meetings. The Editor wishes to assure his readers that these occasional events are not meant in any way to compete with the very important reviews that are regularly published in the *Publications of the Astronomical Society of the Pacific* or in special review publications.

 0004-6256/95/110(4)/1476/16/$0.90

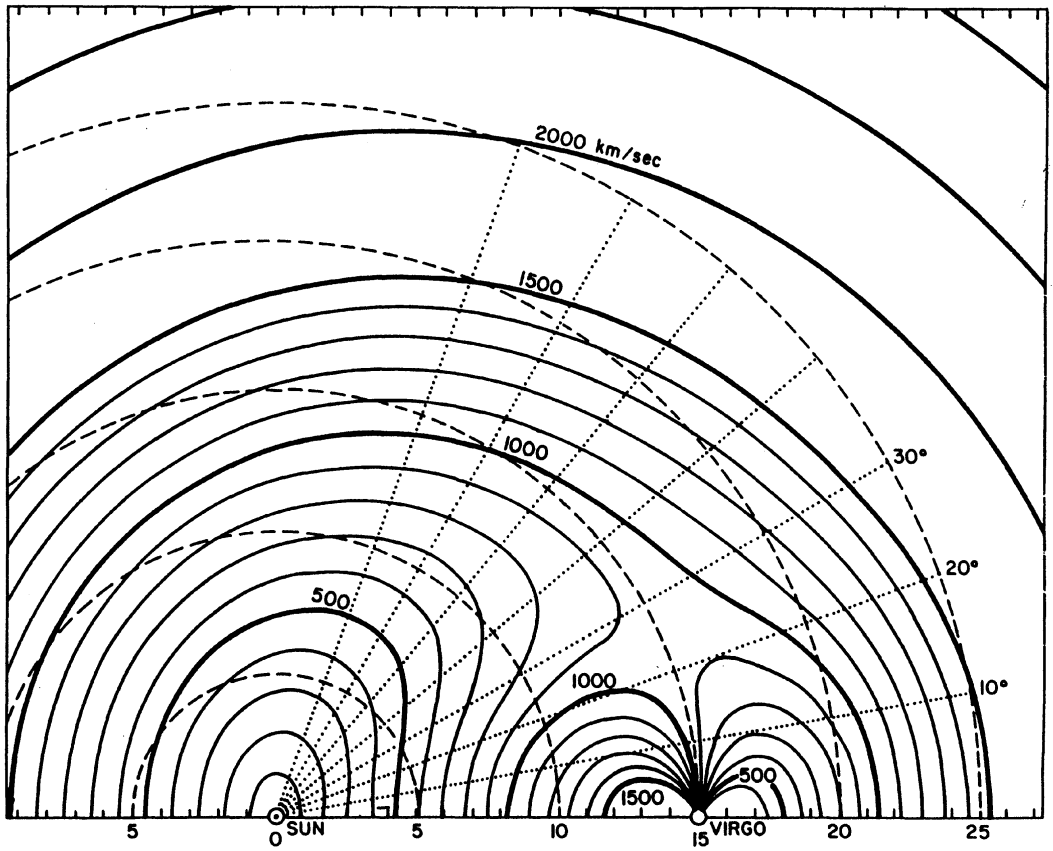

FIG. 1. Model of the local velocity field from Tonry & Davis (1981). The distortions are due to Virgo-centric infall. Dashed lines show the velocity field expected for a pure Hubble flow.

Kennicutt (Co-PI), B. Madore, J. Mould (Co-PI), A. Saha, and P. Stetson. Postdocs and students who have been involved with various aspects of the project are F. Bresolin, L. Ferrarese, M. Han, P. Harding, R. Hill, M. Kelson, M.-G. Lee, R. Phelps, D. Rawson, S. Sakai, N. Silbermann, and A. Turner.

2. THE GROUND-BASED DISTANCE LADDER

2.1 Nature of the Problem

To determine H_0 one needs to measure precise distances to galaxies that are sufficiently distant so that local perturbations to their radial velocities are negligible. The difficulty of this task is demonstrated by Fig. 1, which shows a model of the local radial velocity field from Tonry & Davis (1981). The heavy lines are contours of constant radial velocity as measured from the Local Group, projected to the supergalactic plane. If the Hubble flow were perfectly uniform these contours would be semicircles centered on the Sun, as indicated by the dashed contours, but the actual velocity field is highly distorted, due to the retardation of the cosmic expansion within the Virgo supercluster. The distortions in velocity amount to many tens of percent near the Virgo cluster, and even at 2000 km s^{-1} there are *systematic* deviations at the 10%–25% level. Consequently, if we are to measure H_0 to an accuracy of 10%, we need to extend the distance scale to velocities of 5000–10 000 km s^{-1}, or distances of order 100 Mpc.

Extending the distance scale to such remote galaxies requires at least two steps in the extragalactic distance ladder. Ground-based observations of Cepheid variables, the most reliable primary distance indicator, have a practical limit of a only a few Mpc (Madore & Freedman 1991; Jacoby *et al.* 1992). Although dedicated campaigns with ground-based 4 m class telescopes have yielded candidate Cepheids in more distant galaxies, including two Cepheids in M101 (Cook *et al.* 1986; Alves & Cook 1995), and three candidates in the Virgo cluster spiral NGC 4571 (Pierce *et al.* 1994), these measurements have proven to be extremely difficult and expensive in telescope time. As a result, precise ground-based Cepheid distances remain limited to galaxies within 4 Mpc (see Table 1 in Jacoby *et al.* 1992), more than an order of magnitude short of the distance needed to reliably sample the Hubble flow. Bridging this "twilight zone" requires the application of one or more "secondary" distance indicators, which are calibrated locally then used to extend the distance scale to the 100 Mpc range (Sandage 1958; Sandage & Tammann 1974).

Although *HST* greatly extends the range of direct Cepheid-based distances, it cannot yet reach the region of Hubble flow with Cepheids alone, so a reliable suite of secondary indicators remains a vital part of the H_0 calibration. The strategy adopted by the Key Project is to tie an *HST*-based local Cepheid scale to several (largely ground-based)

secondary indicators to provide a rigorous determination of H_0 and its associated uncertainty.

2.2 Secondary Distance Indicators

One of the biggest success stories in this field in the past decade has been the development or refinement of several superb secondary distance indicators. An excellent review of this subject is given by Jacoby *et al.* (1992, hereafter referred to as J92). It includes detailed descriptions and assessments of several distance indicators and a complete bibliography. An abbreviated summary is given below, with special emphasis on those indicators which are most relevant to the Key Project.

Aaronson & Mould (1986) and J92 define several criteria which the ideal distance indicator should satisfy: (1) it should exhibit a small, quantifiable dispersion, i.e., it is a reliable standard candle. (2) It should be measurable in enough galaxies so that it can be calibrated locally, and its intrinsic dispersion and systematic variation can be tested. (3) It should have a well defined physical basis. (4) It should be luminous enough to be useful at large distances, preferably into the region of Hubble flow. Several indicators which meet these criteria are now available and are described below. Five of these—the infrared Tully–Fisher relation, the planetary nebula luminosity function, surface brightness fluctuations of galactic spheroids, the expanding photosphere method for Type II supernovae, and the peak luminosity of Type Ia supernovae—have been targeted by the Key Project for improved Cepheid-based calibrations.

Infrared Tully–Fisher Relation (IRTF). The Tully–Fisher (TF) method exploits the correlation between H I linewidth (or rotation velocity) and luminosity for spiral galaxies. It was first applied extensively by Tully & Fisher (1977), and extended to infrared wavelengths by Aaronson, Mould, Huchra, and collaborators. Thanks to several large H I and Hα surveys, TF distances are now available for $\gtrsim$2000 field and cluster spirals, extending to velocities of $>$11 000 km s^{-1} (e.g., Aaronson *et al.* 1986; Mathewson *et al.* 1992). The basis of the method rests on the flat rotation curves of spirals, which produce well defined circular velocities and sharply bounded H I velocity profiles; the physical origin of the $L \sim V^4$ scaling law is less well understood (e.g., Burstein 1982), but it appears to be a general property of galaxies. The largest uncertainties associated with the method are a small number of calibrating galaxies, an uncertain intrinsic dispersion, and possible systematic variations with galaxy type and location. These uncertainties have led to debate over the susceptibility of the method to Malmquist biases and other selection effects in distant IRTF samples (Sec. *3.2*).

D_n–σ Relation. This is the dynamical analog of the Tully–Fisher relation as applied to elliptical galaxies or spiral bulges. It has been applied most extensively by the "7 Samurai" collaboration, as discussed in Faber *et al.* (1989) and J92. The indicator has a relatively high dispersion, $\pm$0.52 mag or $\pm$27% in distance for a single galaxy, so the method works best in rich groups or clusters where several galaxies can be observed at once.

Surface Brightness Fluctuations (SBF). This is a quantitative application of the classical criterion of resolution, as developed by Tonry and collaborators (Tonry 1991; J92). The relevant observable is the normalized variance in photon flux for a region of a galaxy, which is determined by the moments of the stellar luminosity function and the distance. It has been applied to elliptical galaxies, S0 galaxies, and spiral bulges, where the fluctuation signal is dominated by individual red giant stars. Comparisons of fluctuation distances for galaxies in nearby clusters show that the intrinsic dispersion is very low, $\pm$0.08–0.15 mag in the *I* band (Tonry 1991). The observed fluctuations are in qualitative accord with expectations from models of old stellar populations (Tonry *et al.* 1990), providing a physical foundation for the technique. In good seeing conditions the method can be applied to galaxies at redshifts of $\sim$4000 km s^{-1} (Tonry 1995), and with *HST* it should be possible to apply it well beyond 10 000 km s^{-1}. Hence this method satisfies our criteria for an optimal secondary indicator. The chief uncertainties are the zero point calibration, which rests on only a handful of nearby galaxies, and corrections for color effects, which presumably reflect sensitivities to age, metallicity, and/or IMF variations (J92).

Planetary Nebula Luminosity Function (PNLF). This method, developed by Jacoby, Ciardullo, and Ford, utilizes observations of the luminosity function of PNe measured in the [O III] λ5007 emission line (Jacoby *et al.* 1989; J92). The PNLF shows a sharp upper cutoff, which can be understood physically as arising from the sharp decline in post-AGB lifetime with increasing stellar core mass, combined with a strong coupling between the [O III] PN flux and the central star luminosity (O^{++} is a strong nebular coolant). The method has been applied mainly to elliptical and S0 galaxies and spiral bulges, but the PNLF appears to be virtually type independent (J92). Comparisons of distances derived for early-type galaxies in groups or the Virgo cluster yield an internal dispersion of $\leqslant$0.10 mag over a large range of luminosity, color, and metal abundance, making this one of the most precise distance indicators available. As with most methods the zeropoint calibration rests on a small number of nearby galaxies, though this situation is improving rapidly (Soffner *et al.* 1995). Other uncertainties discussed by J92 include the uncertain physics of the phenomenon, the occasional presence of overluminous PNe, and metallicity effects. The method also has the most limited range of the indicators considered here, with the most distant targets to date being the Virgo and Fornax clusters. Hence it cannot yet be applied into the region of Hubble flow, though it should be possible to extend further with 8 m class telescopes or *HST*. It already provides a powerful complement to Cepheids as a distance indicator in the 0–20 Mpc range, especially for early-type galaxies where classical Cepheids cannot be observed.

Expanding Photosphere Method for Type II Supernovae (EPM). This is a refinement of the Baade–Wesselink method as applied to the expanding envelopes of Type II supernovae (SNe II). It was first applied by Kirshner & Kwan (1974), and refined most recently by Schmidt, Eastman, Kirshner, and collaborators. Descriptions of the method can be found in Schmidt *et al.* (1994) and references therein (it is not discussed in J92). The method uses spectral fits to the color

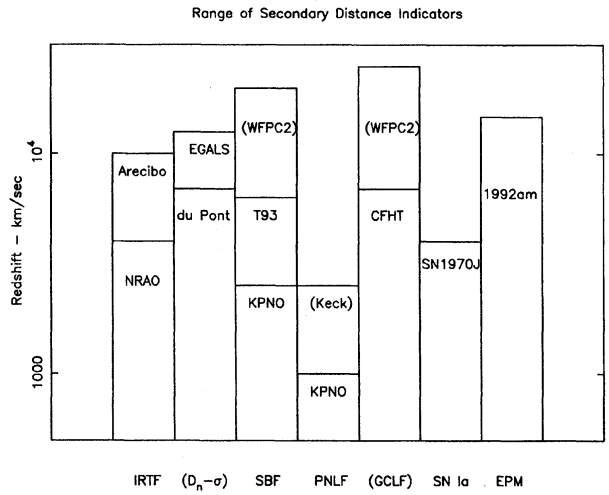

FIG. 2. Histogram showing the approximate limits for the secondary distance indicators discussed in Sec. 2.2. Note the logarithmic velocity scale.

temperature, flux, and radial velocity of the SN envelope vs time to determine the SN distance directly. In principle this technique can be used to measure H_0 independently of the classical distance ladder, but in practice the method requires precise modelling of the substantial dilution effects from scattering in the SN atmospheres, and the results have been checked against observations of SNe in galaxies of known distance. Hence it is treated operationally as a secondary indicator in the Key Project. The internal dispersion of the method is typically ± 0.3 mag (Schmidt *et al.* 1994; Kirshner 1995), which is adequate to determine H_0 if a large sample is observed. One of the main advantages of the method is the large distances over which it can be applied, already to 14 600 km s^{-1} (Schmidt *et al.* 1994). The primary uncertainties are the uncertain zero point calibration of the method (i.e., few SNe II of known distance to check the method), and extinction in some heavily reddened objects.

Peak Luminosities of Type Ia Supernovae (SN Ia). The Hubble diagram for distant SNe Ia shows a low dispersion, of order ± 0.2–0.7 mag, depending on the selection criteria and range of galaxy types considered (e.g., Branch & Tammann 1992; J92). The relatively low dispersion and the large distance range of the SNe Ia make this a very attractive method, and it has received considerable attention, including a dedicated Cepheid calibration program with *HST* (Sandage *et al.* 1994). The SN Ia light curves are thought to be driven by the radioactive decay of ^{56}Ni and ^{56}Co, so the narrow dispersion in peak luminosities presumably is related to the range of exploding stellar core masses. However, the details of the explosion mechanism are not well understood, and it is not yet certain whether the SNe Ia are a homogeneous population with a single well defined peak luminosity. The primary empirical uncertainties at present are the small number of calibrators and possible dependences on light curve shape, spectral type, and/or host galaxy type (Sec. 3.2).

Globular Cluster Luminosity Function (GCLF). The peak luminosity of the GCLF also shows great promise as a standard candle, and the method has been applied by several workers, most notably Hanes, Harris, Baum, and collaborators (cf. J92). The chief advantages of the method are the potential range over which it can be applied (up to 50 Mpc from the ground and $\geq$200 Mpc with *HST*) and a low dispersion, ± 0.3 mag for a single galaxy (Harris *et al.* 1991; J92). However, this method has not yet been applied as extensively as the others, and J92 list several potential error sources which need to be addressed, including the zero point calibration, type and metallicity dependences, and observational errors associated with fitting the peak of a broad GCLF. Given these uncertainties the method is not targeted for calibration by the Key Project, but it is being applied in other *HST* programs (e.g., Baum *et al.* 1994).

Novae. The peak luminosity vs decline rate relation for novae has been applied as a distance indicator by several investigators, as discussed in J92. Novae are sufficiently bright that they should be observable to very large distances, but major uncertainties in the calibration of the method, the time-intensive nature of the observations, and possible confusion of novae with other variables have limited the applicability of the method (J92).

Direct Approaches to Measuring H_0. Several efforts are under way to develop methods which directly measure distances to galaxies or clusters in the region of Hubble flow, independent of the local distance ladder. These do not relate directly to the Key Project, but for completeness we briefly describe the most promising of these methods, gravitational lenses, the Sunyaev–Zeldovich (SZ) method, and masers.

An angular diameter distance to a gravitational lens can be determined directly if one can measure the time delay between variations in the lensed images of the background quasar, as well as the velocity dispersion of the lensing object. The prototype system for this application is Q0957 +561, which has yielded estimates of H_0 in the range 37–70 km s^{-1} Mpc^{-1} (Narayan 1991; Bernstein *et al.* 1993, and references therein). Current constraints on the delay time, velocity dispersion, and lens model are insufficient to tightly constrain H_0, but this may improve with further observations of this and other systems. The SZ method uses measurements of the density of the hot gas in clusters from x-ray emission and Compton scattering of the microwave background radiation to infer the absolute size (and hence distance) of the gas (e.g., Birkinshaw & Hughes 1994). Applications to different clusters currently yield a very wide range of velocity/distance ratios, but improvements in submillimeter instrumentation and the modelling of the cluster gas should improve the precision of the method substantially. Another promising technique uses the measured proper motions and radial velocities of circumnuclear water masers to measure geometric distance to galaxies, as demonstrated in spectacular fashion in the nearby spiral NGC 4258 (Miyoshi *et al.* 1995). This method has enormous potential if it can be applied in more distant galaxies.

Any of these direct methods has the potential for measuring H_0 free of the hierarchy of local distance indicators. Even if this were accomplished, however, it will not diminish the need for a set of well calibrated local distance indicators which can be used to measure the structure and dynamics of the local universe, and to provide accurate distances to nearby galaxies.

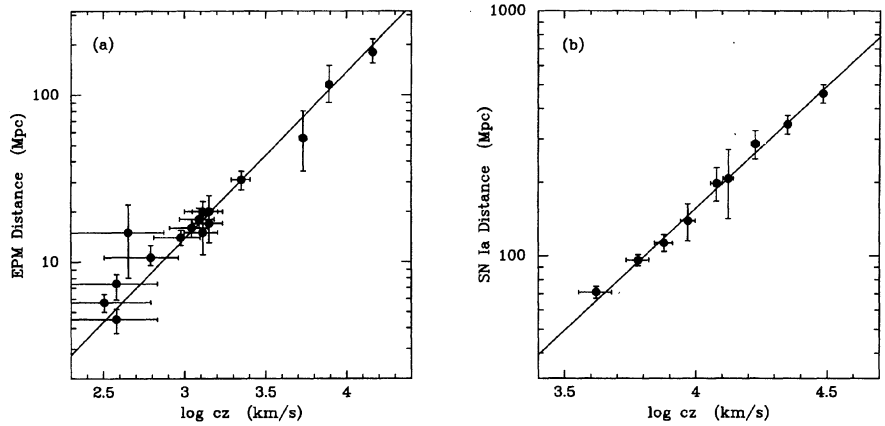

FIG. 3. Velocity–distance relations for SNe II, using the EPM method (Schmidt *et al.* 1994), and SNe Ia, corrected for the luminosity vs decline rate relation, using data from Hamuy *et al.* (1995). Lines indicate the best fitting Hubble laws. Zero point uncertainties are not included in the error bars.

2.3 Discussion

Taken together the secondary indicators discussed above offer a powerful probe of the distance scale and velocity field, extending well into the region of Hubble flow. This is summarized in Fig. 2, which shows the distance limits for each of the techniques; the lower bars indicate limits already achieved, while regions in parentheses indicate limits which can be reached with new instrumentation. Figures 3 and 4 illustrate the current state of the art for the five methods which are most relevant to the Key project. Figure 3 shows the velocity–redshift relations for hosts of SNe II (EPM) and SNe Ia (corrected for the decay rate dependence), using data taken from Schmidt *et al.* (1994) and Hamuy *et al.* (1995), respectively. The solid lines in each plot indicate the expected slope for a linear expansion; note that zero point uncertainties in each method are not included in the error bars shown. The most distant objects measured in these studies are in excess of 30 000 km s^{-1} for the SNe Ia and 14 000 km s^{-1} for the EPM method. Figure 4 compares distances derived for galaxies, groups, or clusters in common using the PNLF vs SBF methods (Ciardullo *et al.* 1993) and the EPM vs Tully–Fisher methods (Schmidt *et al.* 1994; also see Pierce 1994). A more comprehensive comparison of different methods can be found in J92.

These examples show that the requisite level of relative precision has been reached by several secondary indicators, extending in most cases well into the region of linear Hubble flow. The results demonstrate that what has long been regarded as the most difficult step in the distance scale problem—the bridging of the twilight zone—has largely been achieved with these superb data.

3. RESULTS: HOW ACCURATELY IS H_0 DETERMINED?

Given the wealth of data that is now available from the various secondary distance indicators, it is legitimate to ask why the distance scale problem remains unsettled? To address this question it is useful to place the recent observations in the context of previous work. Figure 5 shows a compilation of H_0 determinations in the refereed literature for the period 1975–1995. Each point represents a single paper; to be included the paper had to quote both a value and uncer-

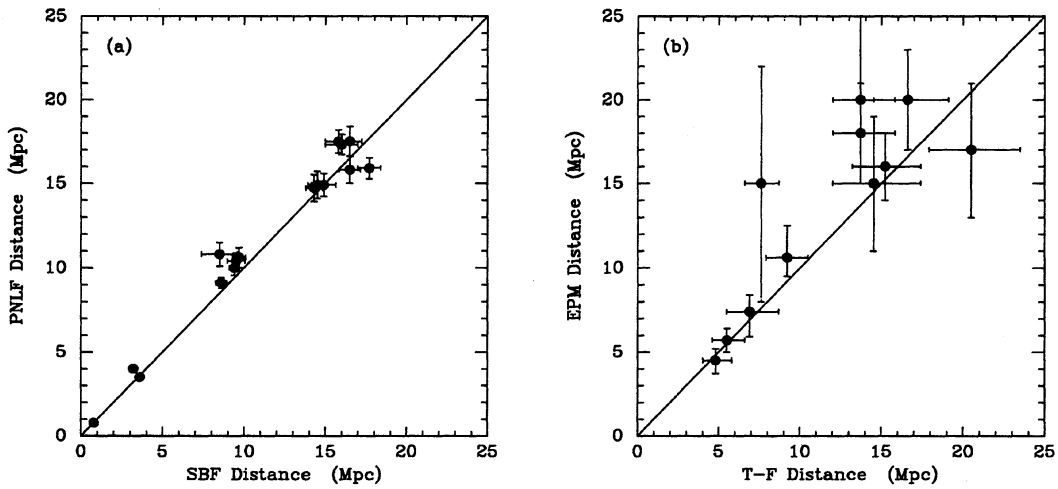

FIG. 4. Comparison of distances derived from SBF, PNLF, TF, and EPM techniques. Data in (a) and (b) taken from Ciardullo *et al.* (1993) and Schmidt *et al.* (1994) respectively.

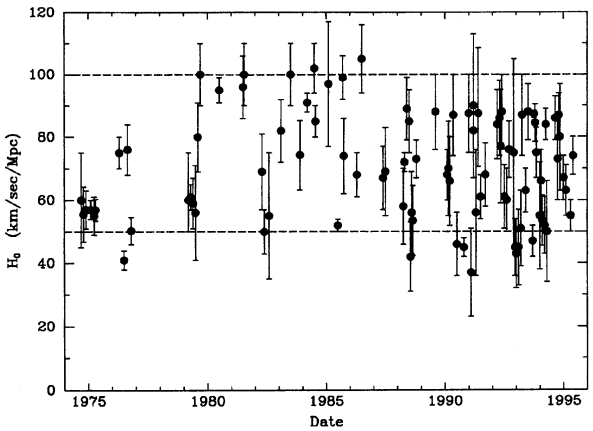

FIG. 5. Determinations of H_0 in the referred literature since 1975. Error bars indicate uncertainties as quoted in the respective papers.

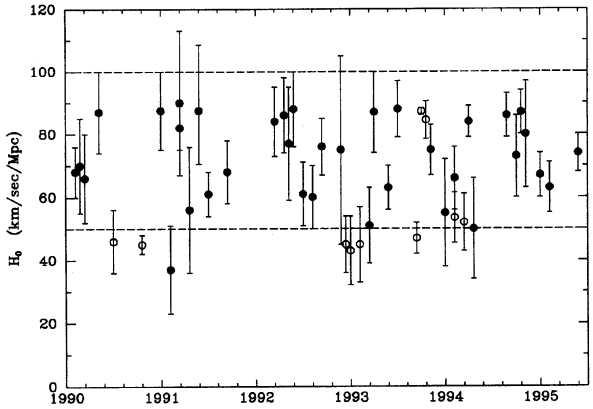

FIG. 6. Same as Fig. 5, but showing papers published since 1990. Open symbols denote papers published by de Vaucoleurs or Sandage and collaborators.

tainty in H_0. An expanded version of this plot, showing papers published since 1990, is shown in Fig. 6. These figures provide some insight into the many popular myths and paradoxes which permeate this field:

"Most measurements of H_0 fall into one of two groups, the long scale ($H_0 \simeq 50$) or the short scale ($H_0 \simeq 100$)." Once true, but less so today. During the early 1980's, when the long series of papers by de Vaucouleurs and Sandage & Tammann dominated the literature, most published values of H_0 fell in the ranges 90–110 or 50–60 km s^{-1} Mpc^{-1}, respectively. The twofold discrepancy between the long and short scales was attributable to several factors: large differences in the corrections for Virgo-centric infall, systematic differences in galactic extinction corrections, and significant differences in the primary and secondary distance scales. In the past decade the discrepancies in the local distance scales and extinction have diminished, many more methods are available, and published values of H_0 now cover a nearly continuous range of 45–90 km s^{-1} Mpc^{-1}.

"The quoted errors in individual measurements of H_0 are almost always smaller than the dispersion of different measurements." Correct. The discrepancy was most blatant in the early 1980's, when the short and long scales differed by several standard deviations, but even today the range of published values is larger than the typical quoted uncertainty. For example the rms dispersion in H_0 values plotted in Fig. 6 is ±26%, whereas the average rms uncertainty quoted in the papers is only ±15% (±11 km s^{-1} Mpc^{-1}). Similar effects can be seen in Figs. 3 and 4, where the systematic differences between secondary methods are often larger than the internal dispersions of the individual techniques (cf. J92).

"If only Dr. _____ would stop publishing papers on H_0 the controversy would be over!" Myth. Perhaps the most widely misunderstood aspect of the distance scale problem. The fallacy of the notion is easily seen in Fig. 6, where we have coded with open circles the papers by the most renowned protagonists of the long and short scales, Allan Sandage and Gerard de Vaucouleurs (and their collaborators). These papers certainly tend to bracket the range of published values, but the remainder of the community is nearly as divided. If one excludes from the distribution the papers of these authors (only as a hypothetical exercise!), the dispersion of H_0 values does decrease, but the median values and (rms) dispersion change by much less than one might expect, from 70^{+17}_{-20} to 75^{+12}_{-15} km s^{-1} Mpc^{-1}.

A comparison of the distance scale compilation of Sandage & Tammann (1995) with those of Jacoby *et al.* (1992), van den Bergh (1992), and de Vaucouleurs (1993) isolates the specific points of disagreement. There is a 17% discrepancy in the cosmological redshift of the Virgo cluster, and large differences in the estimated dispersion of the Tully–Fisher relation, and hence in the corrections for Malmquist bias that must be applied (cf. Sandage 1988; Pierce & Tully 1988; J92). Sandage & Tammann (1995) also attach heavy weight to methods which tend to yield lower values of H_0 (SN Ia, galaxy diameters, SZ), while ignoring methods such as SBF and PNLF which have consistently yielded higher values of H_0. Proponents of the short scale on the other hand place heavy weight on methods such as Tully–Fisher, SBF, PNLF, SN II, GCLF, and D_n–σ, while dismissing as imprecise some of the methods favored by Sandage & Tammann (1995) such as Sc I luminosities and diameters of M31 and M101 "lookalikes."

In view of these results, how accurately is H_0 known today? The unweighted averages quoted above are virtually meaningless, because Figs. 5 and 6 include a mix of good and bad data, and entire sets of measurements may be afflicted with systematic errors. (Many of the unrealistically small error bars shown in Figs. 5 and 6 result from improper application of the central-limit theorem to multiple measurements that contain correlated errors.) However, we *would* maintain that the dispersion of values in Fig. 6 probably offers a more honest assessment of the current uncertainty in H_0 than the typical errors which are quoted in these papers. If one accepts this premise then current ground-based observations constrain H_0 to ±20%–25%, or perhaps ±30%–40% if the full range of values in Fig. 6 is considered. Many authors have maintained that H_0 is already known to <10% uncertainty, and that the controversy is over, but this argument can only be made by selectively excluding a subset of the literature, and by ignoring the basic uncertainties which still plague the local distance scale. Our goal should be to

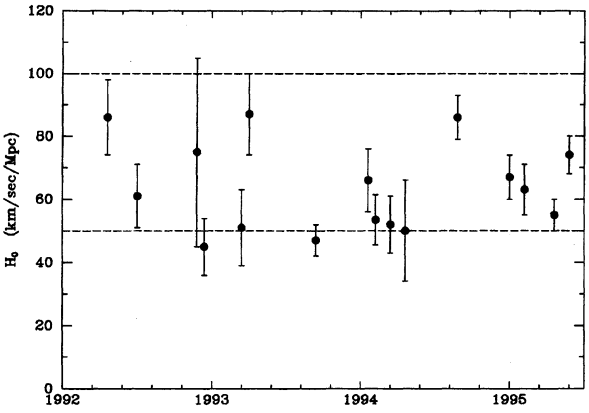

FIG. 7. Determinations of H_0 since 1992, all using the SN Ia peak luminosity method.

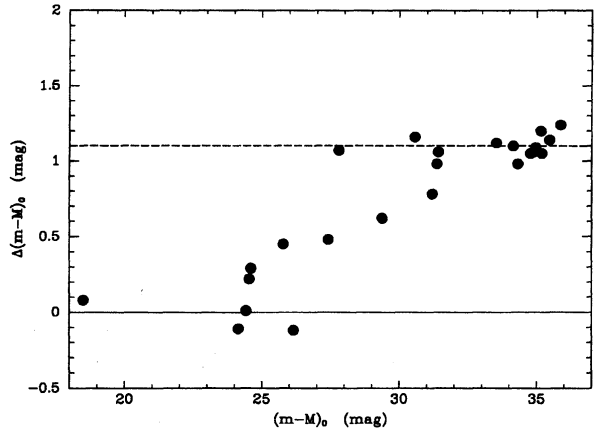

FIG. 8. Difference in distance moduli between long and short scales, plotted as a function of average modulus. See text for references.

construct a distance ladder that is robust enough so that these kinds of subjective value judgements are no longer part of the cosmological debate.

How can H_0 be this uncertain, when the secondary distance indicators appeared to be more precise? The most likely explanation to this paradox is a problem with the zero point calibrations of one or more of the secondary candles. Although most of the secondary methods provide *relative* distances that are accurate to ±10%–20% or better (e.g., Figs. 3 and 4), the zero point calibrations of these methods are based on only 1–7 objects, so systematic errors in the overall scales cannot be ruled out.

The Tully–Fisher method offers a prime example of this problem. The current IRTF calibration rests on only five galaxies with Cepheid distances, among them only two luminous spirals, M31 and M81 (Freedman 1991). The scatter in this five-point IRTF relation is very small, only ±0.16 mag (±8% in distance); however, much larger samples of spirals in nearby clusters show much higher dispersions, up to ±0.4–0.7 mag in the visible (Pierce & Tully 1988; Kraan-Korteweg *et al.* 1988; Sandage 1988). These higher dispersions may well be artifacts of depth or contamination problems in the cluster samples, but we cannot yet rule out the possibility that the five local calibrators underrepresent the true scatter of the relation. Another recent study of the IRTF relation in the Coma cluster region by Bernstein *et al.* (1994) shows a scatter which is nearly as low as for the local calibrators (±0.20 mag), but with a different slope. The uncertainty over the scatter and slope of the TF relation has fueled debate over whether large Malmquist corrections need to be applied to TF distances (e.g., Sandage 1988; J92; Willick 1994), or whether the TF relation has a varying form in different environments (Bernstein *et al.* 1994). To address these questions we need a much better local calibration of the relation.

The situation with the other secondary methods is no better. The EPM method as applied by Schmidt *et al.* (1994) was checked against only three SNe II of known distance (in the LMC, M81, and M101), and only two are consistent with the calibration. The peak luminosities of SNe Ia are calibrated with only two galaxies, both measured recently with *HST*. The SBF method is calibrated with three galaxies (M31, M32, NGC 205), all based on the Cepheid distance to M31 (the recent Key Project distance to M81 adds another point). The PNLF calibration is more secure, with seven calibrators (including two Key Project galaxies), but this still is less than optimal. The shortage of calibrators also makes it difficult to test for possible systematic effects in the methods. For example, the PNLF, SBF, SN Ia, and GCLF methods are calibrated in spiral or irregular galaxies but mainly applied in elliptical and S0 galaxies, leaving their application vulnerable to systematic biases with parent galaxy type. Internal comparisons of distant group and cluster samples can constrain the magnitude of such effects (cf. J92), but the dearth of calibrating galaxies leaves room for considerable uncertainty.

The recent literature on SNe Ia offers an excellent case study in the practical consequences of these calibration uncertainties. Over the past three years this method alone has been applied in 16 papers by ten sets of authors; the resulting values of H_0 are shown in Fig. 7. The large scatter in results, H_0=45–87 km s^{-1} Mpc^{-1}, is all the more remarkable given that most of them are based on nearly the same parent sets of SN Ia observations, but with different calibrations and analysis techniques. In this case the uncertainty can be attributed almost entirely to the poor calibration, which currently rests on only two objects, SN 1937C in IC 4182 and SNe 1972E (and possibly SN 1895B) in NGC 5253. To complicate matters further, the SN Ia luminosity appears to vary systematically with light curve decay rate, and the two calibrating SNe lie near one extreme of the decay rate relation (Phillips 1993; Hamuy *et al.* 1995). The SNe Ia illustrate how uncertainties in the local calibrating distance scale can dominate the error in H_0.

Consequently, the main uncertainty in the current distance scale lies not at large distances, where the secondary indicators give relatively consistent results, but at small distances—just beyond the limit of ground-based Cepheid observations. This can be seen directly in Fig. 8, which shows the discrepancy between the long and short scale distance moduli for galaxies and clusters, plotted as a function of average distance modulus, based on data from Aaronson *et al.* (1986), Sandage & Tammann (1990), van den Bergh

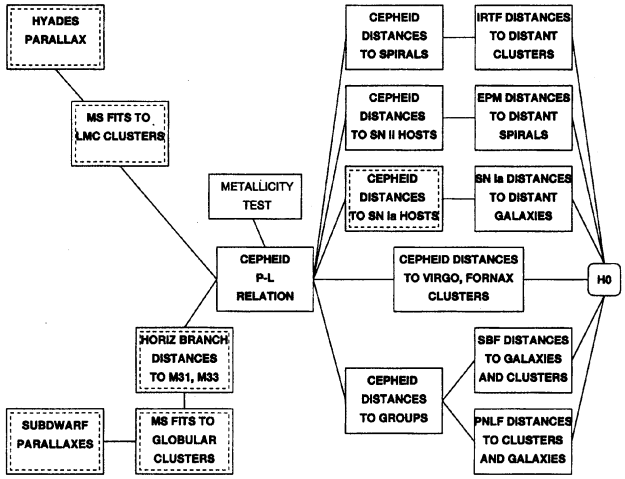

FIG. 9. Flow chart summarizing the *HST* Key Project strategy. Boxes with dashed insets denote observations being carried out by other groups. Application of secondary indicators (rightmost boxes) is mostly based on existing ground-based data.

TABLE 1. *HST* Cepheid target galaxies.

Galaxy	Type	Cycle[c]	IRTF	PNLF	SBF	EPM	SN Ia	Cluster
NGC 925	SBc II-III	4	×	(×)	(×)	(×)		
NGC 1365	SBbc I	5	×	(×)	(×)		(×)	(×)
NGC 1425	Sb II	6	×	(×)	(×)		(×)	(×)
NGC 2090	Sc II	5	×					
NGC 2541	Sc III	5	×	(×)	(×)			
NGC 3031	Sb I-II	1	×	×	×	×		
NGC 3198	Sc I-II	5	×					
NGC 3319	Sc II-III	6	×					
NGC 3351	SBb II	4	×	(×)	(×)			
NGC 3368[a]	Sab II	4	×	(×)	(×)			
NGC 3521	Sbc II-III	6	×					
NGC 3621	Sc II.8	4	×					
NGC 4321	Sc I	4		(×)	(×)	×	(×)	(×)
NGC 4414	Sc II.2	4	×	(×)	(×)		×	
NGC 4496[b]	SBc III-IV	4					×	
NGC 4535	SBc I.3	6	×	(×)	(×)		(×)	(×)
NGC 4536[b]	Sc I	4	×				×	
NGC 4548	SBb I-II	6	×	(×)	(×)		(×)	(×)
NGC 4639[b]	SBb II	5	×	(×)	(×)		×	(×)
NGC 4725	Sb II	5	×	(×)	(×)			
NGC 5253[b]	Amorphous	3					×	
NGC 5457	Sc I	3,4	(×)			×		
NGC 7331	Sb I-II	4	×		×	×		
IC 4182[b]	Sm IV-V	1					×	
UGC 5889[a]	Sm V	4		(×)	(×)			

[a]Part of separate GO program by Tanvir *et al.*.

[b]Part of separate GO program by Sandage *et al.*.

[c]Galaxies in future cycles tentative.

(1992), and de Vaucouleurs (1993). The scales are roughly consistent within about 3 Mpc, where the distance scale is anchored by Cepheid variables and/or RR Lyrae stars. This high degree of consistency in the local distance scale is a relatively recent development, and largely owes to refinements in the observation of Cepheids in nearby galaxies over the past decade, including corrections to scale errors of up to 0.5 mag as a result of CCD photometry, corrections for reddening as a result of infrared photometry, the ability to test for metallicity effects, and cross comparisons with other techniques such as RR Lyrae stars, SN 1987A, and the tip of the red giant branch, which taken together lend confidence to the use of Cepheids as accurate distance indicators (Madore & Freedman 1991; J92). Figure 8 also shows that the long and short scales are in good *relative* agreement at the largest distances, beyond the Virgo cluster. The nearly twofold divergence between the long and short scales occurs in the ~3–20 Mpc range.

This problem is an unavoidable byproduct of the limited range of ground-based Cepheid measurements. The 3–4 Mpc volume which is accessible from the ground contains only a few luminous galaxies, mostly late-type spirals, and too few to properly calibrate any secondary distance indicator. It is this aspect of the distance scale problem that has been revolutionized by *HST*. With *HST* we can measure precise Cepheid distances to virtually any spiral or irregular galaxy located within 30 Mpc, offering a thousandfold increase in the accessible volume, encompassing the entire local supercluster. The key to solving the H_0 problem lies in combining *HST*'s unique capability for extending the primary distance scale with the superb ground-based secondary distance scale.

4. THE *HST* KEY PROJECT

4.1 Objectives and Strategy

We have seen that the most critical missing element in the distance scale is a set of primary distances to galaxies in the 3–30 Mpc range. *HST* will address this problem directly by measuring precise Cepheid distances to ~25 galaxies with redshift velocities <2000 km s^{-1}. These galaxies will serve as benchmarks within the local supercluster, which can be used in future programs to calibrate any number of secondary distance indicators. The Key Project sample has been specifically designed to strengthen the zero point calibrations of five secondary distance indicators, which can be applied in turn to determine H_0 to an accuracy of ±10%, including internal and systematic errors. Observations are being obtained over a three-year period beginning in 1994, and will eventually involve ~300–400 h of spacecraft time.

Figure 9 summarizes the strategy of the Key Project, and Table 1 lists the galaxies tentatively targeted for Cepheid observations. Crosses denote galaxies that directly calibrate a secondary candle, while crosses in parentheses denote indirect calibrations via group or cluster membership. Table 1 includes galaxies being observed in the Key Project as well as smaller samples which are being observed by other teams headed by A. Sandage and N. Tanvir. Table 1 also lists the approximate observing schedule by *HST* cycle; future assignments (Cycle 6) are tentative.

The core of the Key Project sample is a set of 18 inclined spirals which have been selected as optimal calibrators for the IR Tully–Fisher relation. When combined with ground-based Cepheid surveys of local galaxies ($d \leq 3$ Mpc) the number of IRTF calibrators will be increased from 5 to nearly 30, and will include a wide range of types (Sb–Irr) and luminosities ($-M_B \sim 16$–22). The spiral sample was also selected to strengthen the zero point calibrations of other secondary indicators. For example four of the spirals are hosts to well measured SNe II, and a fifth lies in the same group as a SN II host. This will increase the number of EPM calibrators from one object (SN 1987A) to six. Cepheid observations of at least five SN Ia hosts are being carried out in a separate *HST* Cepheid program headed by Sandage, and those observations will be incorporated into the Key Project along with our data for another SN Ia host. The PNLF and SBF methods are applied to elliptical and S0 galaxies, which do not contain classical Cepheids, but we will measure ~14

spirals which lie in groups or clusters containing PNLF and SBF calibrators. Depth effects within groups and clusters diminish the accuracy of these calibrations, but the additional data will roughly double the number of calibration points and provide an external check on the existing zero points of these important secondary methods.

With the improved Cepheid-based calibrations in hand, each of the secondary indicators can then be used to measure H_0 independently (the PNLF method only reaches the Virgo and Fornax clusters, so corrections for peculiar velocities are required in that case). The dispersion in the resulting values will then provide an objective estimate of the uncertainty in H_0, above any systematic uncertainties in the Cepheid distances themselves (see below).

In addition, we plan to measure Cepheid distances to five spiral galaxies in the Virgo and Fornax clusters. When combined with the cosmological redshifts of these clusters these distances will provide yet another measurement of H_0. This H_0 value by itself may *not* be accurate to $\pm 10\%$, due to uncertainties from cluster depth effects and corrections for the local velocity perturbations. However, it will provide a single-step *primary* measurement of the Virgo and Fornax distances which bypasses nearly all errors in the secondary distance scale, and as such will serve as a powerful consistency check on the resulting value of H_0.

Any systematic errors in the calibration of the Cepheids themselves will propagate through the entire H_0 determination with full weight, so testing and strengthening the calibration of the $P-L$ relation is another important focus of the Key Project. The current $P-L$ calibration is based on observations of 22 Cepheids in the LMC (Madore & Freedman 1991), assuming an LMC distance modulus of 18.5 ± 0.1 mag. (The galactic $P-L$ relation is less useful because of large uncertainties in the distances to the calibrating variables, and a lack of long-period Cepheids, which are the ones predominantly observed at large distances.) This calibration is subject to uncertainties in the LMC distance, the finite size of the LMC calibrating sample, and any systematic changes in the $P-L$ relation with metallicity.

To improve the accuracy of the Cepheid zero point calibration, a number of complementary programs are being carried out both from the ground and using *HST*. From the ground, new main-sequence *UBVRI* and *JHK* photometry is being obtained for Cepheids in galactic clusters and the Pleiades (in collaboration with Eric Persson). Ultimately, a direct calibration of and distance to the LMC will be obtained based on new distances and reddenings for galactic Cepheids from near-infrared photometry. These results will serve as one external check on the current adopted distance to the LMC. *BVRIJHK* data are also being obtained for the current calibrating sample of Cepheids in the LMC. At the same time, the sample of stars in the LMC with *V* and *I* (as well as *JHK*) photometry is being extended to a sample of about 100 stars. Searches are underway for Cepheids in the Sculptor group galaxies NGC 247 and NGC 7793 (Freedman *et al.* 1995), two additional calibrators for the Tully–Fisher relation.

A thorough recalibration of the local distance ladder is being undertaken with *HST*, as summarized on the left side of Fig. 9. Astrometric observations of the Hyades and solar neighborhood subdwarfs will tighten the calibration of the Population I and II main sequences. Main sequence fitting of intermediate-age clusters in the LMC, and horizontal branch fitting of globular clusters in M31 and M33, both based on *HST* photometry, will provide improved Cepheid-independent distances to those galaxies. Most of this work is being carried out by other groups outside the Key Project, as indicated by the dashed boxes in Fig. 9. Combining these results with the measured Cepheid samples in the LMC, M31, and M33 will provide three calibrating galaxies for the $P-L$ relation, and independent Pop I and Pop II checks on the zero point. This should provide an objective external measure of the uncertainty of the entire Cepheid ladder.

TABLE 2. Estimated uncertainties in secondary zero point calibrations.

Parameter		IRTF	PNLF	SBF	EPM	SN Ia
σ/galaxy[a]	(mag)	0.40	0.15	0.15	0.32	0.36
N		30	18	17	6	11
σ/N^{a}	(mag)	0.07	0.04	0.04	0.13	0.11

[a]Does not include group and cluster depth effects, which may increase net dispersions for PNLF and SBF methods slightly.

Metallicity effects are another source of systematic error. Fortunately, the most recent theoretical calculations predict only a mild dependence, 0.1 mag in the *I* band between $Z=0.04$ and $Z=0.001$ (Chiosi *et al.* 1993). However, it is important to perform an empirical test, because the typical spiral galaxy in the Key Project is considerably more metal-rich than the LMC Cepheids which calibrate the $P-L$ relation. A first test of this effect was carried out by Freedman & Madore (1990) for M31. Based on *BVRI* photometry of Cepheids obtained in three fields at different radial distances from the center of M31, these authors found a small (0.27 mag) difference in distance modulus between the inner and outermost fields in M31, where the metal abundance is estimated to range over a factor of 4–5. This difference is slightly larger than can be attributed to observational uncertainty alone, but is consistent with the mild dependence predicted at *I* by Chiosi *et al.* Follow-up *JHK* data have been obtained in these fields to further constrain the level to which abundance effects may affect the Cepheid zero point. As part of the Key Project we are conducting a further empirical test by observing two Cepheid fields in the nearby spiral M101. The mean abundances in these fields bracket the range of metallicity in the Key Project sample, and if a significant metallicity effect is present we will be able correct for it using H II region abundances which have been obtained for the *HST* fields (Zaritsky *et al.* 1994).

The error budget for entire distance scale chain is summarized in Tables 2 and 3. Table 2 shows the expected uncertainties in each of the secondary scales; listed are a conservative estimate of the internal dispersion per galaxy (cf. J92), the number of calibrating galaxies, and the net uncertainty. An additional allowance needs to be made for systematic differences between different methods (J92). This can only be tested when all of the methods have been fully calibrated, and for now we apply a conservative estimate of ± 0.10 mag to the overall secondary scale. Table 3 lists the total error

TABLE 3. Key Project error budget.

Error source	Modulus uncertainty (mag)
LMC distance	±0.10
P-L calibration	±0.07
Cepheid extinction	±0.10
Secondary methods[a]	±0.10
Velocity field	±0.05
Cumulative uncertainty	±0.19

[a]Including systematic differences between methods (J92).

budget, adding errors in the Cepheid zero point, uncertainty introduced by the finite number of calibrating Cepheids, extinction, and an allowance for residual systematic errors from velocity perturbations in the 5000–10 000 km s^{-1} frame (Lauer & Postman 1994). The combined uncertainty from all of these sources is ±0.19 mag, or 9% in H_0. The actual errors may differ from these allowances, of course, but Tables 2 and 3 demonstrates that a 10% measurement of H_0 is feasible with an *HST* sample of ~25 galaxies. It also shows how difficult it becomes to reduce the uncertainty below the ±10% level. Errors in the Cepheid ladder alone limit the precision of *all* current distance scale calibrations to no better than ±6%–7%, so any claims that H_0 has been measured to higher accuracy are unrealistic.

4.2 Observing Strategy: Cepheids with HST

HST has several attributes that make it uniquely suited for measuring Cepheid distances to galaxies. The most obvious advantage is the 0.″1 resolution (the pixel size on the Wide Field Camera, which is used for most of the observing). In these galaxies the detectability of faint stars is limited not by photon statistics but rather by crowding from the semiresolved stellar background in the disk. Most of the Cepheids discovered to date by *HST* are in the range $V \leqslant 27.5$, considerably brighter than *HST*'s limiting magnitude for isolated point sources, but 3–4 mag fainter than is practical from ground-based telescopes (e.g., Pierce *et al.* 1994).

Equally important for measuring Cepheids are the optimized scheduling and repeatability of the observations. Cepheid monitoring programs traditionally have been multiyear (or multidecade) campaigns, with large blocks of telescope time allocated during successive dark runs over these periods. The limited depth of the ground-based imaging (especially with photographic plates) was partly responsible for this slow progress, but an equally serious problem has been period aliasing from gaps in temporal coverage and variations in the quality of the photometry from epoch to epoch. Weather, lunar phases, and seasonal cycle introduce aliases on scales of order of a few, 10, and 100 d respectively, and these are critical for measuring periods of luminous extragalactic Cepheids, most with periods in the 10–60 d range.

These problems are virtually eliminated with *HST*. The telescope can observe the same position at identical orientations for a window of ~40–70 d, depending on the position and spacecraft orientation constraints. This allows us to define an optimal series of exposures which fully samples a given range of Cepheid periods with a minimum of overhead. Such a strategy was developed by Barry Madore and Wendy Freedman for the Key Project. Currently we obtain 12 epochs which are spaced in a power-law series, with the longest spacing set by the orientation window, and the shortest ranging from 1–4 d, depending on the shortest periods we expect to detect. Simulations showed that 12 optimally scheduled epochs provided excellent phase coverage of Cepheids with $P = 10$–60 d, with only modest improvements as more observations were added (Freedman *et al.* 1994a). This minimum redundancy approach makes the most efficient use of the precious *HST* resources, and was critical to making a Key Project of this scope feasible.

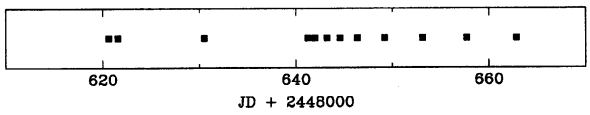

FIG. 10. Diagram showing the temporal coverage of 12 *HST* observations of M81.

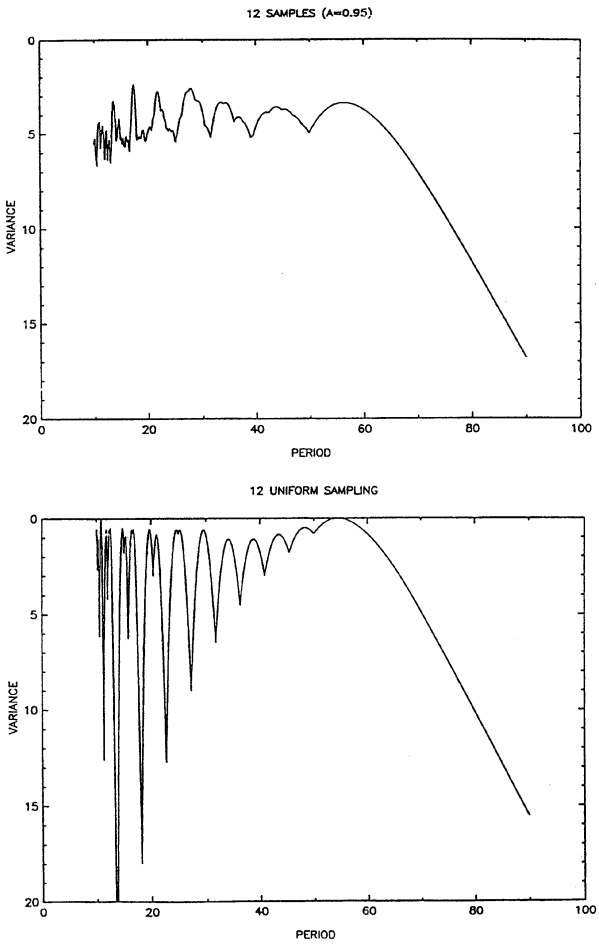

FIG. 11. Sampling variance of Cepheid light curves plotted as a function of Cepheid period, using the M81 sampling shown in Fig. 10 (left) and equally spaced observations over the same 45 d window (right), from Freedman *et al.* (1994a). The structure in the latter plot shows the effects of period aliasing, which is virtually eliminated with the minimum redundancy logarithmic sampling (left).

The sampling strategy was first tested on two fields in M81, which we observed in 1992 when the *HST* spherical aberration limited us to nearby target galaxies. We obtained data at 12 epochs distributed over a 45 d window, as is shown in Fig. 10. The sensitivity of this sampling strategy is illustrated in Fig. 11, which plots a variance statistic measuring the probability that a randomly phased Cepheid would be identified with the correct period, as determined from Monte-Carlo simulations. Figure 11 compares this variance as a function of Cepheid period for our actual M81 spacings (left) with what would have been obtained for 12 uniformly spaced epochs over the same 45 d window (right). The large negative spikes in the latter plot are due to period aliases—periods which cannot be unambiguously identified due to resonances between the Cepheid period and the sampling interval. Figure 11 shows that these aliases are largely eliminated by the power-law sampling, at the expense of a modest loss of completeness at all periods. The efficacy of this technique was confirmed with the successful detection of 31 Cepheids in the two *HST* fields (Freedman *et al.* 1994a, b), notwithstanding the small effective aperture of the aberrated *HST*($\sim$1 m), the limited sampling, and the restricted field coverage. For comparison, a 35 yr ground-based campaign on the Hale 5 m telescope, begun by Hubble and completed by Sandage (1984), yielded only two Cepheids with unambiguous periods. It is the combination of *HST*'s unique capabilities, its resolution, its optimized scheduling, and the repeatability of its photometry that make it so ideally suited to this problem.

This sampling strategy is now being applied to all of the galaxies in the Key Project survey. Each series of observations consists of 16 cosmic-ray split exposures spaced over 45–70 d, 12 epochs in V (F555W), which are used to determine periods and mean visual magnitudes, and 4 epochs in I (F814W). The V band is optimal for detecting Cepheids with *HST*, because the amplitude of variation increases at shorter wavelengths, while detector efficiency, Cepheid brightness, and reddening all degrade shortward of V. An additional epoch one year later is obtained to resolve aliases in the original series and to identify long-period variables. At I the amplitude is a factor of two smaller than at V (so that fewer observations are needed to determine mean magnitudes), and the V and I observations together provide information on reddening (see below).

4.3 Data Analysis

Reducing these data presents a unique set of challenges: a typical V exposure contains 10^4–10^5 stars, so analyzing a full 32 exposure data set (two exposures for each of the 12 V and 4 I epochs) typically entails over a million photometric measurements. Most fields contain of order 10–100 Cepheids, or $\sim 10^{-4}$ of the sample. The photometry and variable star identification routines must be robust against the $\sim 10^6$ cosmic rays contained in a typical data set. The photometry analysis programs must also deal with the severe stellar crowding in the resolved disks of the galaxies, with images which severely undersample the instrumental point spread function (PSF).

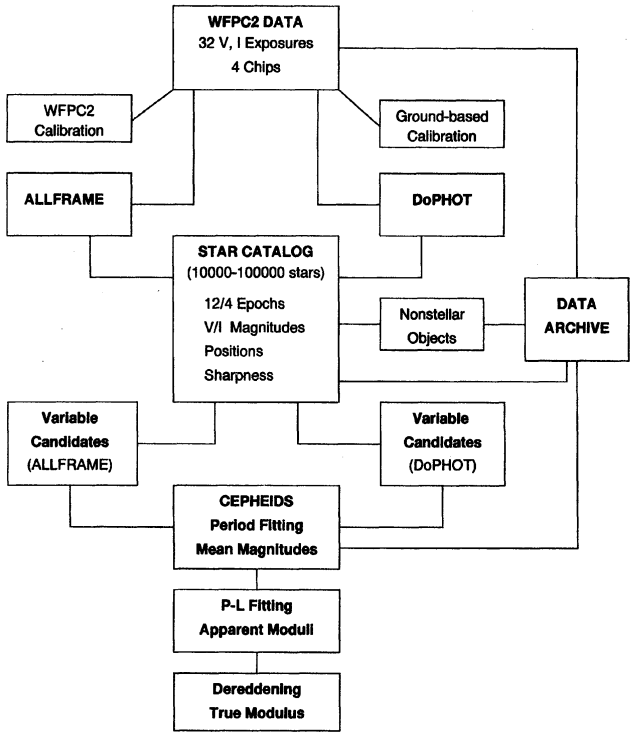

FIG. 12. Flow chart summarizing data analysis for *HST* photometry in the Key Project.

To deal with the volume and difficulty of the stellar photometry we designed a double-blind reduction pipeline, with nearly all of the critical analysis tasks performed by separate groups utilizing different analysis packages. A chart summarizing the reduction path is shown in Fig. 12. This double-blind approach was developed initially as a check on the reduction algorithms themselves, but we have adopted it permanently as a safeguard against reduction errors and to provide an external check on our measuring uncertainties. Thus, for example, the photometric zero points are currently calibrated using at least two independent sources, including the WFPC2 instrumental calibration and at least one set of ground-based CCD photometry. Likewise, the stellar photometry is performed by at least two groups using different packages (below), and the identification of variable stars and period fitting is done independently by different groups. For the sake of consistency the final analysis stages, including P–L fitting, dereddening, and distance determination are performed using a common set of algorithms, with a rigorous internal error analysis.

Details of the data analysis methods are described in Freedman *et al.* (1994a), Stetson (1994), Saha *et al.* (1994), and Kelson *et al.* (1995), and are beyond the scope of this review, but a brief mention of the photometry packages may be of general interest. Conventional aperture photometry is virtually useless in these crowded fields, so all of the photometry is performed with PSF-fitting software modelled after the DAOPHOT or DoPHOT packages (Stetson 1987; Schechter *et al.* 1993). These programs were designed for use with fully sampled images, where the fitting algorithms can be applied to utmost advantage. These algorithms break

down in an undersampled images; for example, the PSF of the same star will change depending on whether its image falls in the center of a pixel or on the boundary between two or more pixels. To deal with these problems two modified photometry packages were developed which are optimized for the *HST* data, ALLFRAME, an extension of DAOPHOT written by team member Peter Stetson, and a customized version of DoPHOT written by team member Abhijit Saha. Saha is also a member of the Sandage *et al.* (1994) team, and his program is used by that group.

The operating principles of both programs are similar. Instead of fitting each exposure independently, a master list of stellar positions and magnitudes is generated from a summed and filtered image constructed from all of the exposures. An iterative comparison of each individual frame with the master catalog is then used to compute geometric and photometric transformations to be applied to the entire frame, as well as an independently determined PSF (high order PSF terms are derived from independent observations). This approach preserves the positional information contained in the much higher signal/noise summed exposures, and thus greatly reduces photometric errors due to undersampling or cosmic rays. Stars are subtracted in successive iterations to improve the magnitude and sky background estimates, as in previous versions of these packages. See Stetson (1994) and Saha *et al.* (1994) for details.

The output of these programs is a set of magnitudes and errors for each of the 32 exposures, along with position and image shape information from the master catalog. Variable star candidates are identified by comparing the dispersion in brightness with that of other stars of comparable magnitude, or by an algorithm which compares the dispersion in magnitude between different epochs with the dispersion between different halves of individual cosmic-ray split pairs of exposures (Welch & Stetson 1993). Candidate variables are then inspected visually on the images to confirm the variability and to eliminate false positives caused by semiresolved companions, asterisms, or cosmic rays. The colors of the variables are also checked to ensure that they are consistent with those of (reddened) Cepheids. Periods are determined using a modification of the method of phase dispersion minimization (Laffler & Kinman 1965; Stellingwerf 1978), as described in Freedman *et al.* (1994a). The entire analysis is performed independently using the two photometry packages and variable analysis programs, and a final Cepheid list is obtained by merging these data sets.

The final reduction steps include fitting the observed $P-L$ relation to the LMC calibrating relation in V and I and combining these to derive a reddening-corrected true distance modulus. A number of tests are applied to check for biases in the data set, such as correlating the derived moduli with Cepheid amplitude, presence of nearby companions, or CCD chip, or by fitting the regressions in luminosity or period (e.g., Freedman *et al.* 1994a; Kelson *et al.* 1995). These provide an independent check on the uncertainties in the derived distances. Unresolved companions to the Cepheids can be identified by examining the shapes and amplitudes of the light curves. We are also performing a series of artificial star simulations to quantitatively assess the completeness and susceptibility of the data to contamination. The V and I differential moduli (relative to the LMC) are fitted to the galactic extinction law to derive the true modulus (Freedman & Madore 1990; Freedman *et al.* 1994a). The final distance moduli are subject to errors in the mean magnitudes, uncertainty in the reddenings of the LMC reference sample, the limited $V-I$ wavelength baseline, and the assumption of a galactic reddening law. Together these introduce an uncertainty at roughly the ± 0.1 mag level, making extinction corrections a significant contributor to the total error budget. Eventually this can be improved by observing some of the Cepheids in the J, H, and/or K bands, either with the NICMOS camera on *HST* or possibly with a 8–10 m class telescope from the ground.

4.4 Data Archive

One of the important components of an *HST* Key Project is the establishment of a data archive which can be used by the astronomical community for follow-up studies. Aside from the raw data, which are accessible from the STScI archive one year after observation, the Key Project team plans to release several data products. These will include averaged and cosmic ray filtered images of each field, complete photometric catalogs of stellar and nonstellar objects, and detailed information on the Cepheid variable stars, including finder charts, light curves, and photometric information. The latter are being published in the referred literature for each galaxy, while the former will be available in digital form, once final calibrations are completed. Information on accessing these data will be published in a future team paper.

5. PRELIMINARY RESULTS: M100 AS PROOF OF CONCEPT

As of April 1995 *HST* observations had been obtained for 13 galaxies by three different groups (see Table 1). Reductions for most of these data are ongoing, but distances have been published for four galaxies, IC 4182 (Saha *et al.* 1994), M81 (Freedman *et al.* 1994a), NGC 5253 (Saha *et al.* 1995), and the Virgo cluster spiral M100=NGC 4321 (Freedman *et al.* 1994b). IC 4182, M81, and NGC 5253 were observed prior to the *HST* refurbishment with WFPC1, while the M100 observations were obtained entirely with WFPC2. The M100 results are especially significant, because detecting Cepheids in the Virgo cluster was one of the original design objectives of *HST*, and the success of these observations verifies the feasibility of the overall Key Project strategy.

Figures 13 and 14 show examples of pre-refurbishment observations, when *HST* proved to be effective in identifying Cepheids in nearby galaxies. Figure 13 shows light curves of several Cepheids in the starburst irregular galaxy NGC 5253, part of a total sample of 14 Cepheids identified by Saha *et al.* (1995). This galaxy was host to two SNe Ia, 1972E and 1895B, and is part of the sample being used by Sandage *et al.* to calibrate this secondary indicator. Figure 14 shows

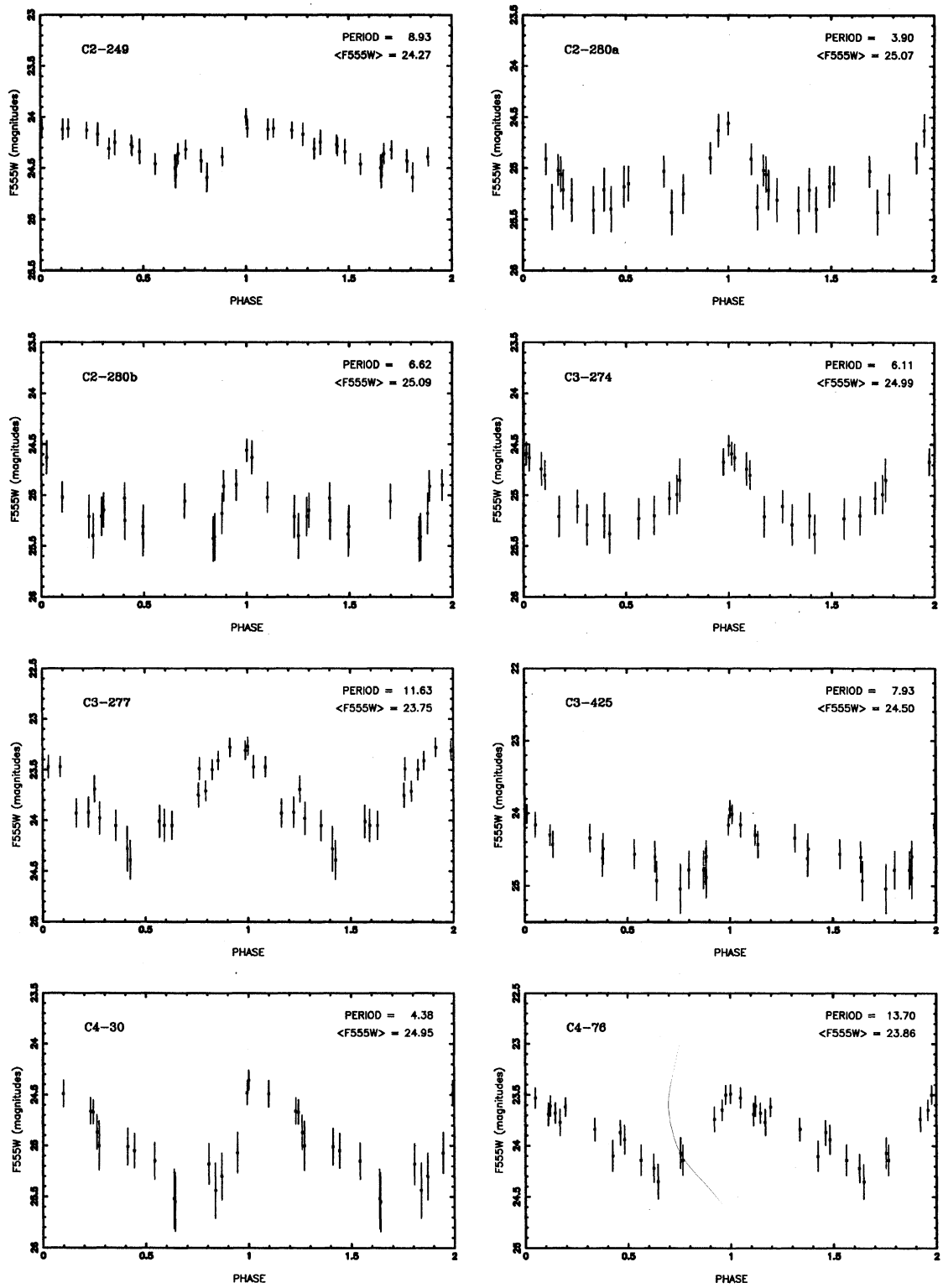

FIG. 13. Sample light curves for Cepheid variables in NGC 5253 observed with WFPC1, from Saha *et al.* (1995).

the $P-L$ relation for two WFPC1 fields in M81, which was observed by the Key Project (Freedman *et al.* 1994a). The outer field in M101 was also observed with WFPC1, and a final analysis of its Cepheids will be published in the near future (Kelson *et al.* 1995).

The performance of the refurbished *HST* with WFPC2 is illustrated in Figs. 15–20. Figures 15 (Plates 58 and 59) show a median averaged image of NGC 925 (Silbermann *et al.* 1994), shown with a ground-based image for comparison (Sandage & Bedke 1988). NGC 925 has a relatively uncrowded low surface brightness disk, and the effects of the increased resolution and depth of *HST* are manifest. Figure

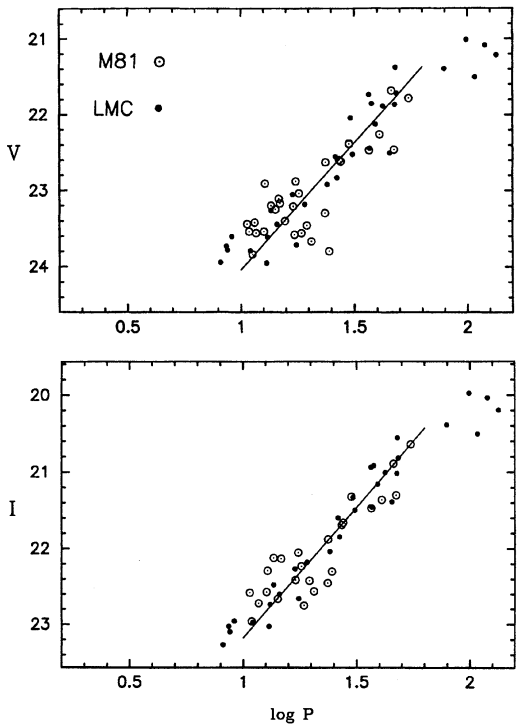

FIG. 14. Period–luminosity relation for Cepheid variables in M81, observed with WFPC1, from Freedman *et al.* (1994a).

16 shows a preliminary $V-I$ color–magnitude diagram of the galaxy from Silbermann *et al.* (1994). Candidate Cepheids are shown as large circles, and their concentration to the instability strip demonstrates the quality and depth of the WFPC2 photometry.

Figure 17(a) (Plate 60) shows a median filtered V image of M100, made from ten 30 min exposures (5 h total), and Fig. 17(b) (Plate 61) shows a high-contrast image of a single CCD field (WF4 to the NE), to provide a better indication of the full depth and resolution of the data. The faintest stars visible in Fig. 17(b) have $V\sim28$. Other notable (and less welcome) features in these images are the crowding in the inner disks and spiral arms, and the prominent dust lanes covering much of the images. Figures 18 and 19 show examples of light curves and a preliminary $P-L$ relation for M100, both from Freedman *et al.* (1994b). In uncrowded fields we obtain reliable photometry to $V\sim27.5$, which implies that we should be able to detect 10 d Cepheids to a limiting distance of ~20 Mpc. If one is willing to restrict the sample to longer period Cepheids it should be possible to reach ~30 Mpc with reasonable exposure times.

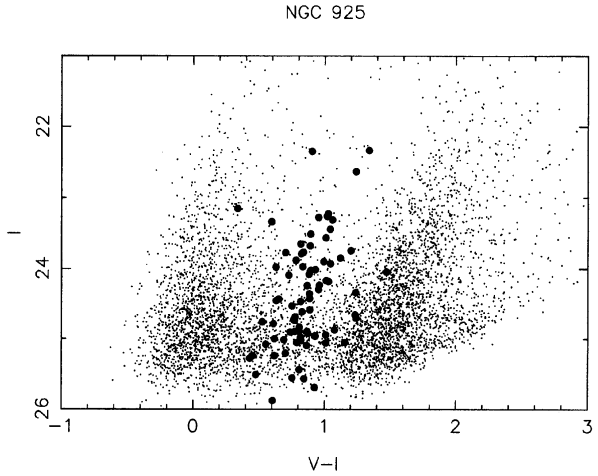

FIG. 16. Preliminary $V-I$ color–magnitude diagram for NGC 925, from Silbermann *et al.* (1994). Large symbols indicate Cepheid candidates, as determined from variability criteria.

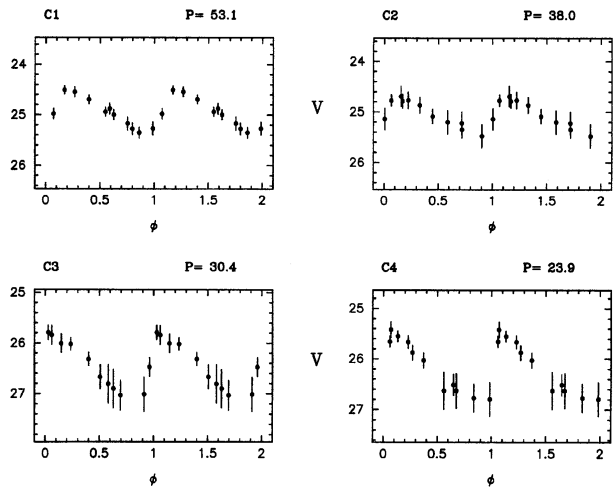

FIG. 18. V light curves for examples of Cepheids in M100, from Freedman *et al.* (1994b).

The $P-L$ relation in Fig. 19 corresponds to a reddening-corrected M100 distance of 17 ± 1.8 Mpc (Freedman *et al.* 1994b). A complete analysis which includes a larger Cepheid sample and improved WFPC2 calibrations is in progress (Ferrarese *et al.* 1995), but our preliminary distance already has interesting implications for H_0, as discussed by Freedman *et al.* (1994b) and Mould *et al.* (1995). If M100 lies at the mean distance of the Virgo cluster, H_0 can be estimated

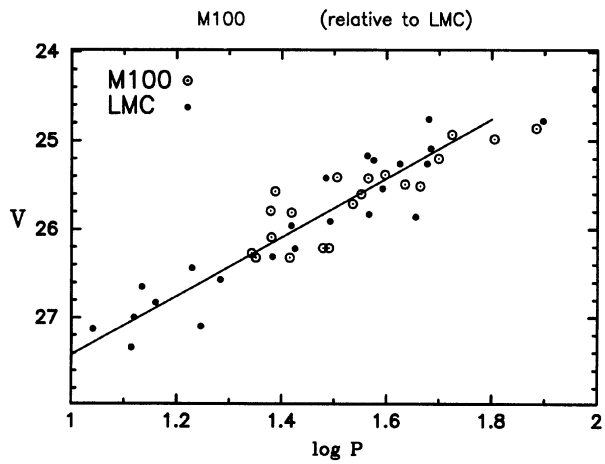

FIG. 19. Preliminary period–luminosity relation for Cepheids in M100, from Freedman *et al.* (1994b).

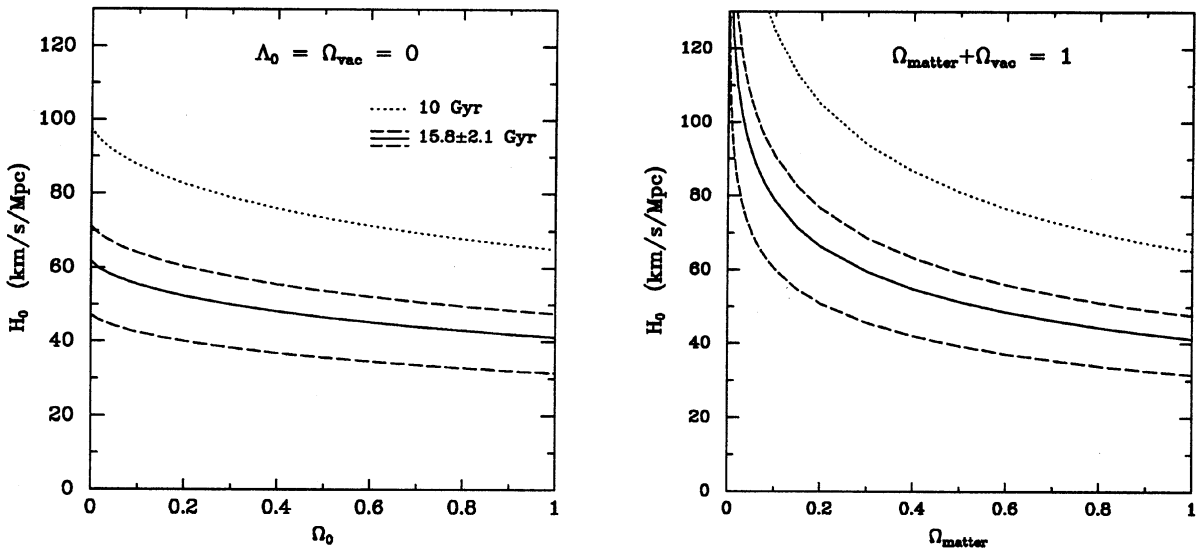

FIG. 20. Relation between H_0, the density parameter Ω_0, and cosmic age for models with cosmological constant $\Lambda=0$ (left), and for flat universes with nonzero cosmological constant (right). The solid and dashed lines indicate an age of 15.8±2.1 Gyr, the best current limits on the ages of the oldest globular clusters. The dotted line shows an age of 10 Gyr for comparison. Our preliminary value of $H_0=80$ km s^{-1} Mpc^{-1} is clearly inconsistent with the globular cluster age scale if $\Lambda=0$, especially for $\Omega\sim1$. However, the second plot shows that the age and expansion time scales can be readily reconciled if $\Omega_{matter}\leqslant0.3$ and $\Omega_{vacuum}\geqslant0.7$. For most realistic values of Ω the Hubble constant must be $\leqslant50$ km s^{-1} Mpc^{-1} to avoid an age conflict in a $\Lambda=0$ cosmology.

in several ways: (1) from the distance and (corrected) velocity of the Virgo cluster itself, (2) from the distance and velocity of the Coma cluster, using several estimates of the Virgo–Coma relative modulus, or (3) by using the Virgo cluster distance to calibrate one or more of the secondary distance indicators. The first two methods yield an approximate value $H_0\simeq80\pm17$ km s^{-1} Mpc^{-1} (Freedman *et al.* 1994b), and similar values are derived from the secondary indicators (Mould *et al.* 1995).

This preliminary result is in best agreement with the short distance scale of Jacoby *et al.* (1992), de Vaucouleurs (1993), and others, but given the large uncertainty values as low as 60 km s^{-1} Mpc^{-1} are not ruled out. The ±20% error estimate is dominated by uncertainty in M100's location in depth with respect to the Virgo cluster core, with smaller contributions from the M100 Cepheid distance itself, the Virgo cosmological velocity, and errors in the secondary distance scale. Our 95% confidence range is 50–100 km s^{-1} Mpc^{-1}. All of these estimates include allowances for systematic errors.

The cosmological implications of values of H_0 in this range have been discussed by numerous authors (e.g., Carroll *et al.* 1992; Fukujita *et al.* 1993; Freedman *et al.* 1994b). Figure 20, adapted from Carroll *et al.* (1992), shows the relationship between H_0, the density parameter Ω_0, and the age of the universe, for cosmological models with zero cosmological constant Λ (left), and on the right for flat models ($\Omega_{total}=1$) with nonzero cosmological constant. The solid and dashed curves show the cosmic age for $\tau=15.8\pm2.1$ Gyr, the best current age estimate for the oldest galactic globular clusters (Bolte & Hogan 1995). The dotted line shows the locus for $\tau=10$ Gyr for comparison. The left panel shows that our estimate of $H_0=80\pm17$ km s^{-1} Mpc^{-1} can be reconciled with a $\Lambda=0$ model only if the matter density of the universe is low ($\Omega\leqslant0.3$) and the estimates of H_0 and stellar ages are pressed to the lower and upper limits of their respective error ranges. On the other hand, if the uncertainties attached to these H_0 and age values prove to be conservative, then *no combination of the parameters* is consistent with a $\Lambda=0$ cosmology. Resolving this age conflict requires either that $H_0\leqslant50$ km s^{-1} Mpc^{-1} for $\tau\sim16$ Gyr, or that the stellar age scale be of order 8–12 Gyr, for $H_0\sim80$ and $\Omega=1$–0.1. It is interesting, however, that a flat universe with finite cosmological constant can accommodate these age and distance scales, if $\Omega_{matter}\leqslant0.3$, as shown in the right panel of Fig. 20.

Figure 20 provides an illuminating illustration of the cosmological implications of a short (or long) distance scale, but it would be premature to draw any firm conclusions from these results. The H_0 range shown is based on Cepheid observations of a single Virgo cluster spiral, and uncertainties in this measurement leave plenty of room for resolving the age conflict. At this preliminary stage we are far from being able to apply any rigorous cosmological test. But we are confident that over the next three years the combination of *HST*'s marvelous capabilities and the superb foundation of ground-based observations will allow us to fix the value of H_0 at last, and the cosmological implications of that result should be unmistakable.

We are indebted to the other members of the Key Project team, who are jointly responsible for many of the results presented in this paper. We thank John Tonry and Nancy Silbermann for providing illustrations used in this paper. It is a pleasure to thank George Jacoby for many stimulating and insightful conversations on the distance scale. The Key Project is supported by NASA through Grant GO-2227-87A.

REFERENCES

Aaronson, M., Bothun, G., Mould, J., Huchra, J., Schommer, R. A., & Cornell, M. E. 1986, ApJ, 302, 536
Aaronson, M., & Mould, J. 1986, ApJ, 303, 1
Alves, D. R., & Cook, K. H. 1995, AJ (in press)
Baum, W. A., *et al.* 1994, BAAS, 26, 1398
Bernstein, G., Tyson, J. A., & Kochanek, C. 1993, AJ, 105, 816
Bernstein, G. M., Guhathakurta, P., Raychaudhury, S., Giovanelli, R., Haynes, M. P., Herter, T., & Vogt, N. P. 1994, AJ, 107, 1962
Birkinshaw, M., & Hughes, J. P. 1994, ApJ, 420, 33
Bolte, M., & Hogan, C. J. 1995, Nature, 376, 399
Branch, D. R., & Tammann, G. A. 1992, ARA&A, 30, 389
Burstein, D. 1982, ApJ, 253, 539
Carroll, S. M., Press, W. J., & Turner, E. L. 1992, ARA&A, 30, 499
Chiosi, C., Wood, P. R., & Capitanio, N. 1993, ApJS, 86, 541
Ciardullo, R., Jacoby, G. H., & Tonry, J. L. 1993, ApJ, 415, 479
Cook, K. H., Aaronson, M., & Illingworth, G. 1986, ApJ, 301, L45
de Vaucouleurs, G. 1993, ApJ, 415, 10
Faber, S. M., Wegner, G., Burstein, D., Davies, R. L., Dressler, A., Lynden-Bell, D., & Terlevich, R. J. 1989, ApJS, 69, 763
Ferrarese, L., *et al.* 1995 (in preparation)
Freedman, W. L. 1990, ApJ, 355, L35
Freedman, W. L., & Madore, B. F. 1990, ApJ, 365, 186
Freedman, W. L., *et al.* 1994a, ApJ, 427, 628
Freedman, W. L., *et al.* 1994b, Nature, 371, 757
Freedman, W. L., *et al.* 1995 (in preparation)
Fukujita, M., Hogan, C., & Peebles, P. E. J. 1993, Nature, 366, 309
Hamuy, M., Phillips, M. M., Maza, J., Suntzeff, N. B., Schommer, R. A., & Avilés, R. 1995, AJ, 109, 1
Harris, W. E., Allwright, J. W. B., Pritchet, C. J., & van den Bergh, S. 1991, ApJS, 76, 115
Jacoby, G. H., Ciardullo, R., Ford, H. C., & Booth, J. 1989, ApJ, 344, 704
Jacoby, G. H., *et al.* 1992, PASP, 104, 599
Kelson, D., *et al.* 1995, ApJ (in press)
Kirshner, R. P. 1995, private communication
Kirshner, R. P., & Kwan, J. 1974, ApJ, 193, 27
Kraan-Korteweg, R. C., Cameron, L. M., & Tammann, G. A. 1988, ApJ, 331, 620
Laffler, J., & Kinman, T. D. 1965, ApJS, 11, 216
Lauer, T., & Postman, M. 1994, ApJ, 425, 418
Madore, B. F., & Freedman, W. L. 1991, PASP, 103, 933
Mathewson, D. S., Ford, V. L., & Buchhorn, M. 1992, ApJS, 81, 413
Miyoshi, M., Moran, J., Hernstein, J., Greenhill, L., Nakai, N., Diamond, P., & Inoue, M. 1995, Nature, 373, 127
Mould, J., *et al.* 1995, ApJ (in press).
Narayan, R. 1991, ApJ, 378, L5
National Academy of Sciences 1969, Scientific Uses of the Large Space Telescope (National Academy of Sciences, Washington)
Phillips, M. M. 1993, ApJ, 413, L105
Pierce, M. J., & Tully, R. B. 1988, ApJ, 330, 579
Pierce, M. J. 1994, ApJ, 430, 53
Pierce, M. J., Welch, D. L., McClure, R. D., van den Bergh, S., Racine, R., & Stetson, P. B. 1994, Nature, 371, 385
Saha, A., Labhardt, L., Schwengler, H., Macchetto, F. D., Panagia, N., Sandage, A., & Tammann, G. A. 1994, ApJ, 425, 14
Saha, A., Sandage, A., Labhardt, L., Schwengler, H., Tammann, G. A., Panagia, N., & Macchetto, F. D. 1995, ApJ, 438, 8
Sandage, A. 1958, ApJ, 127, 513
Sandage, A., & Tammann, G. A. 1974, ApJ, 191, 603
Sandage, A. 1984, AJ, 89, 621
Sandage, A. 1988, ApJ, 331, 605
Sandage, A., & Bedke, J. 1988, Atlas of Galaxies, NASA Publ. SP-496
Sandage, A., Saha, A., Tammann, G. A., Labhardt, L., Schwengler, H., Panagia, N., & Macchetto, F. D. 1994, ApJ, 423, L13
Sandage, A., & Tammann, G. A. 1990, ApJ, 365, 1
Sandage, A., & Tammann, G. A. 1995, in Current Topics in Astrofundamental Physics, edited by N. Sánchez (in press)
Schechter, P. L., Mateo, M., & Saha, A. 1993, PASP, 105, 1342
Schmidt, B. P., Kirshner, R. P., Eastman, R. G., Phillips, M. M., Suntzeff, N. B., Hamuy, M., Maza, J., & Avilés, R. 1994, ApJ, 432, 42
Silbermann, N. A., *et al.* 1994, BAAS, 26, 1353
Soffner, T., Méndez, R. H., Jacoby, G. H., Ciardullo, R., Roth, M. M., & Kudritzski, R. P. 1995, A&A (in press)
Stellingwerf, R. F. 1978, ApJ, 224, 953
Stetson, P. B. 1987, PASP, 99, 191
Stetson, P. B. 1994, PASP, 106, 250
Tonry, J. 1995, private communication
Tonry, J., & Davis, M. M. 1981, ApJ, 246, 680
Tonry, J., Ajhar, E. A., & Luppino, G. A. 1990, AJ, 100, 1416
Tonry, J. 1991, ApJ, 373, L1
Tully, R. B., & Fisher, J. R. 1977, A&A, 54, 661
van den Bergh, S. 1992, PASP, 104, 861
Welch, D. L., & Stetson, P. B. 1993, AJ, 105, 1813
Willick, J. A. 1994, ApJS, 92, 1
Zaritsky, D., Kennicutt, R. C., & Huchra, J. P. 1994, ApJ, 420, 87

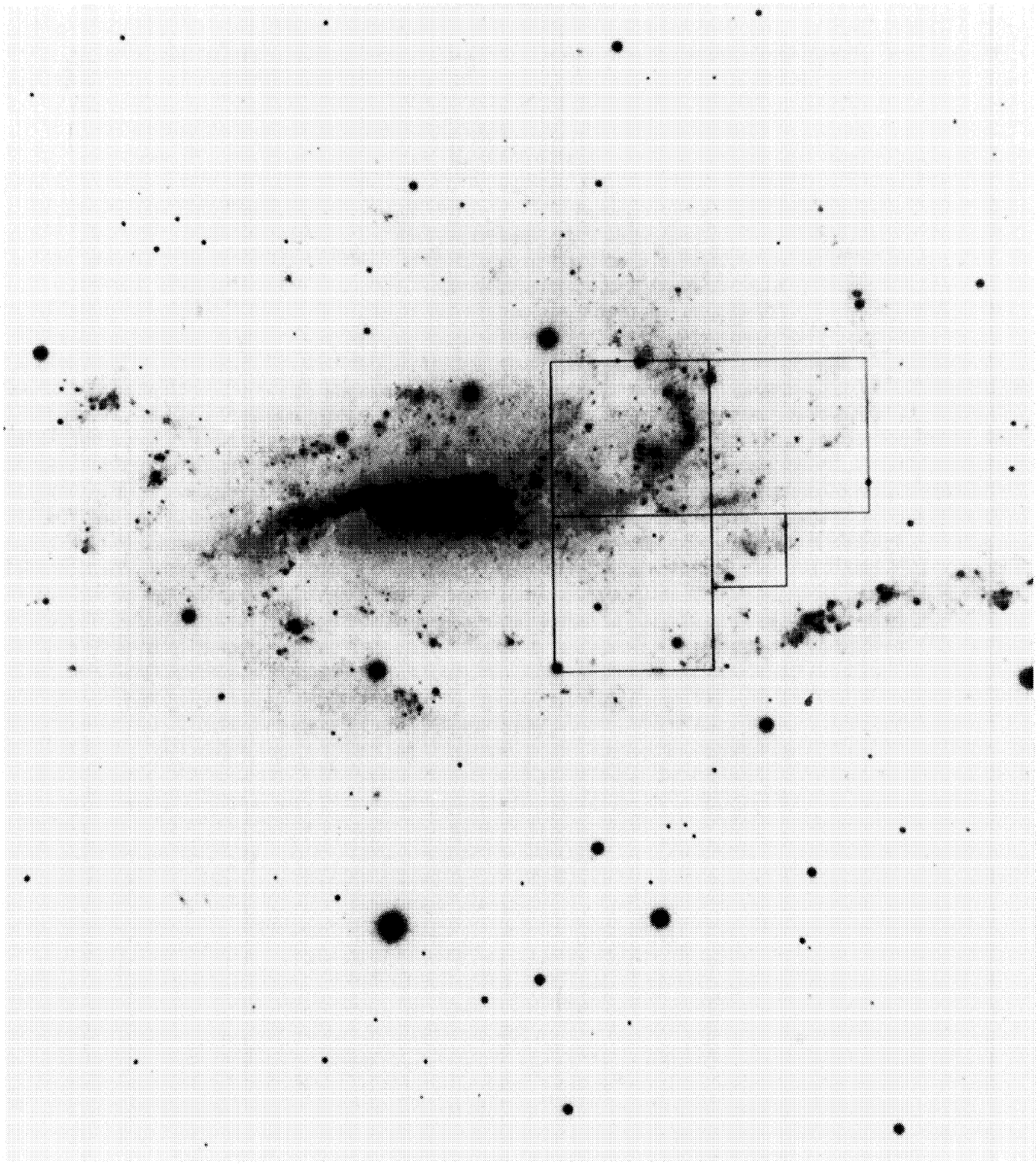

FIG. 15. Comparison of ground-based image of NGC 925 with median averaged WFPC2 exposure. The inset in the ground-based image shows the region observed with WFPC2 by Silbermann *et al.* (1994).

Kennicutt *et al.* (see page 1488)

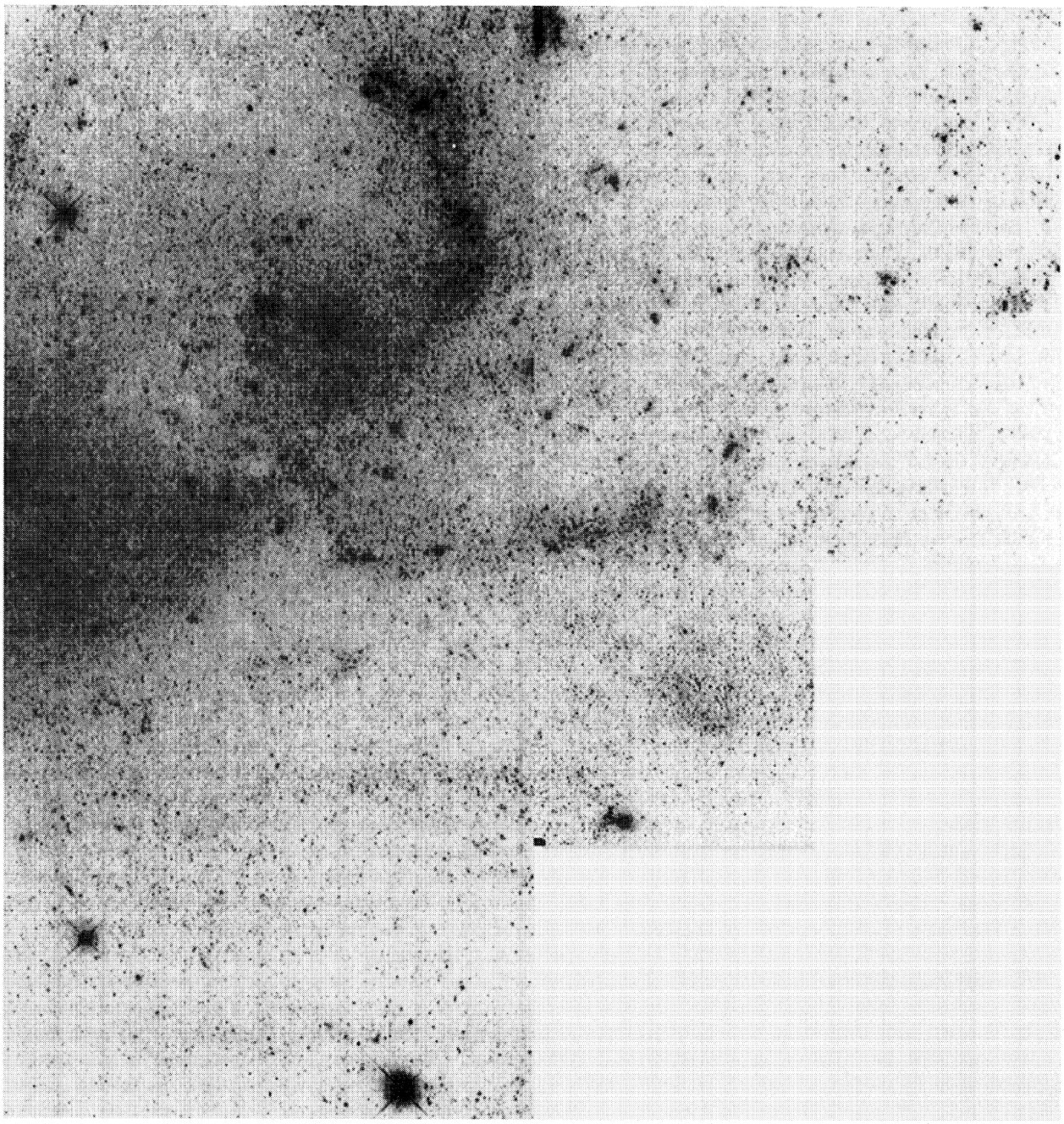

FIG. 15. (continued)

Kennicutt *et al.* (see page 1488)

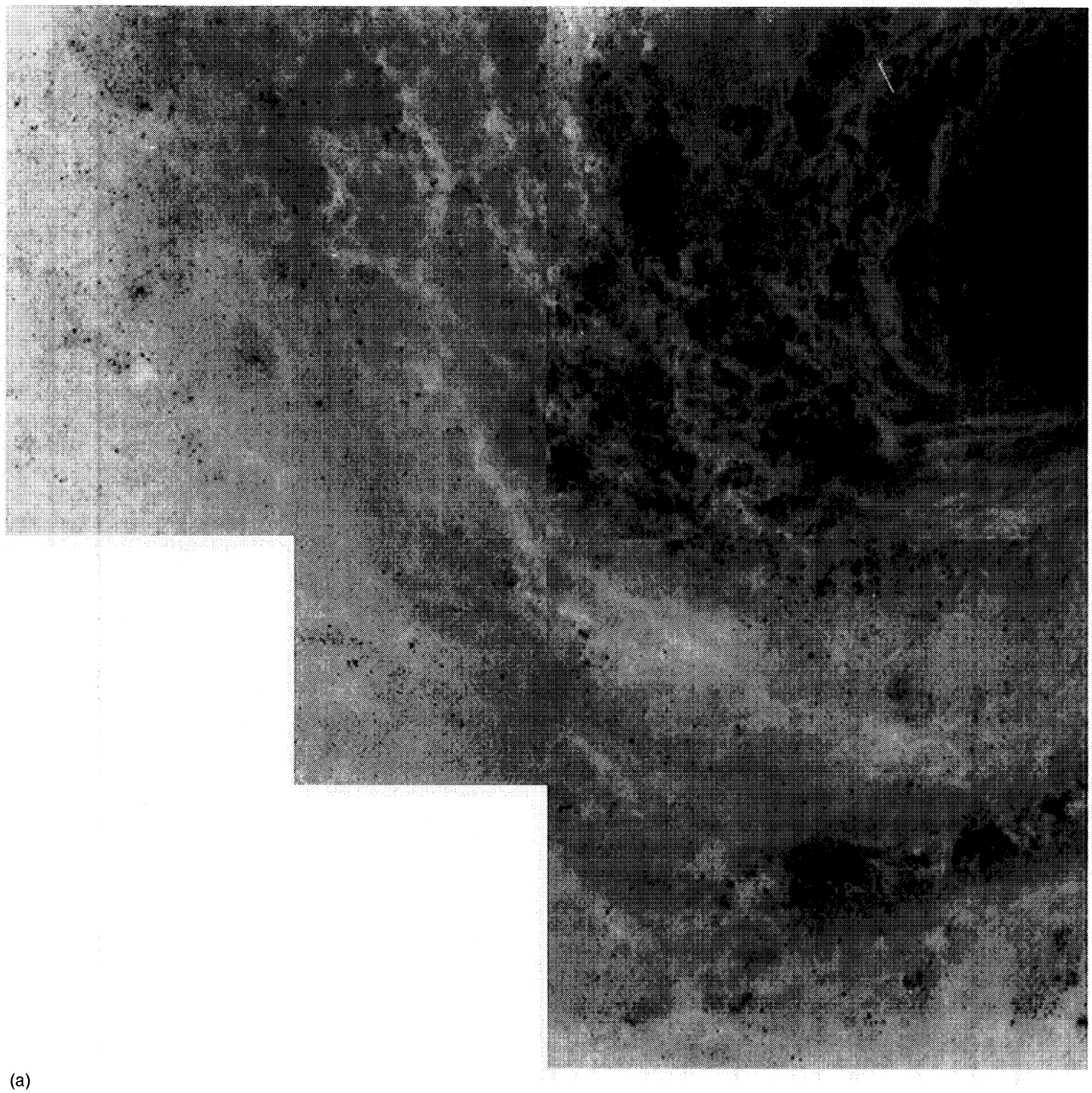

(a)

FIG. 17. (a) Median averaged 5 h WFPC2 exposure of the Virgo cluster cluster spiral M100. (b) High-contrast image of chip WF4.

Kennicutt *et al.* (see page 1489)

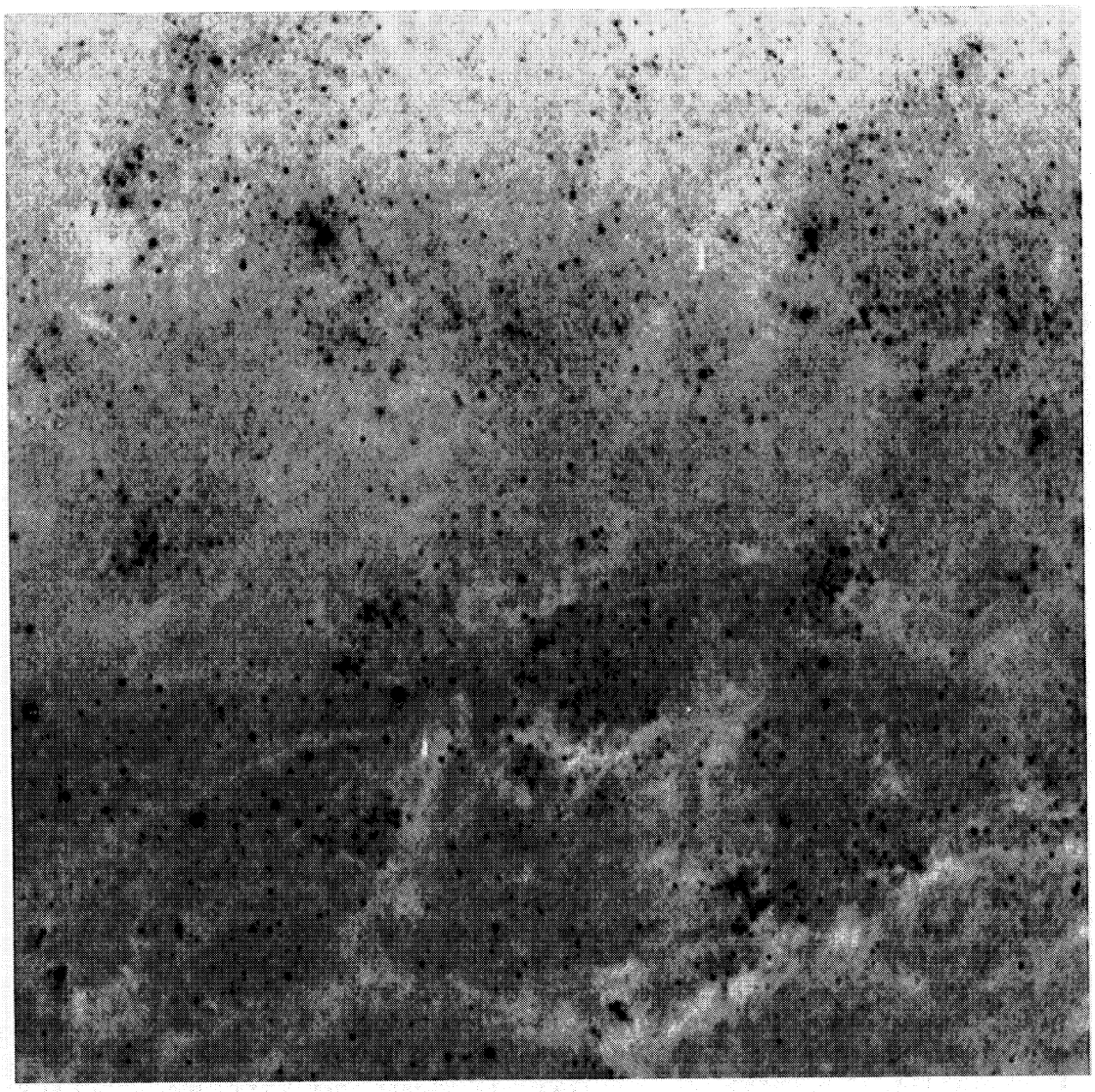

(b)

FIG. 17. (continued)

Kennicutt *et al.* (see page 1489)